Carbohydrate Polymers 87 (2012) 2488–2495

Contents lists available at SciVerse ScienceDirect

Carbohydrate Polymers

journal homepage: www.elsevier.com/locate/carbpol

Cellulose nanocrystals as a reinforcing material for electrospun poly(methyl methacrylate) fibers: Formation, properties and nanomechanical characterization

Hong Dong[a,*], Kenneth E. Strawhecker[a], James F. Snyder[a], Joshua A. Orlicki[a], Richard S. Reiner[b], Alan W. Rudie[b]

[a] U.S. Army Research Laboratory, Aberdeen Proving Ground, MD 21005, United States
[b] USDA Forest Service, Forest Products Laboratory, Madison, WI 53726, United States

ARTICLE INFO

Article history:
Received 21 September 2011
Received in revised form 24 October 2011
Accepted 7 November 2011
Available online 15 November 2011

Keywords:
Cellulose nanocrystals
Nano-DMA
Nanoindentation
Poly(methyl methacrylate) fibers
Electrospinning
Thermal properties

ABSTRACT

Uniform fibers composed of poly(methyl methacrylate) (PMMA) reinforced with progressively increasing contents of cellulose nanocrystals (CNCs), up to 41 wt% CNCs, have been successfully produced by electrospinning. The morphological, thermal and nanomechanical properties of the composite sub-micron fibers were investigated. The CNCs derived from wood pulp by sulfuric acid hydrolysis were well dispersed in solutions of PMMA and the processing solvent *N,N*-dimethylformamide prior to fiber formation. Well-formed fibers with controllable diameters were generated reproducibly at all CNC contents investigated including 41 wt%. The orientation of the CNCs along the fiber axis was facilitated by the electrospinning process and observed directly from microscopy examination. Shifts in thermal transitions of PMMA with increasing CNC content suggest hydrogen bonding interactions between CNC hydroxyl groups and carbonyl groups on the PMMA matrix. Nanoscale dynamic mechanical analysis (nano-DMA) was performed using nanoindentation on single fibers perpendicular to the fiber axis. Many of the current challenges associated with single fiber nanoindentation are addressed, such as fiber diameter range and minimum, depth to diameter ratio, and valid depth range under these experimental conditions. Fibers that contained 17 wt% CNCs showed a modest increase of 17% in the storage modulus of PMMA, a high modulus polymer of interest for transparent composite applications.

1. Introduction

Polymer nanocomposites have been a subject of increasing interest in recent years because of their significantly enhanced mechanical properties and thermal stability versus neat polymers or conventional polymer composites. Incorporation of mechanically robust nanoscale fillers such as nanoclays, graphite nanoplatelets, carbon nanotubes and inorganic nanoparticles into polymer matrices has been extensively exploited (Hussain, Hojjati, Okamoto, & Gorga, 2006). Utilizing cellulose nanocrystals (also referred to as nanowhiskers or whiskers) as a reinforcing phase for developing new nanocomposite materials has been recently investigated, and many efforts focused on dispersion of hydrophilic cellulose nanocrystals into hydrophobic polymeric matrices (Eichhorn et al., 2010). Cellulose nanocrystals (CNCs) as a reinforcing phase have several advantages over other types of nanofillers, as they are easily modified, inexpensive, renewable and biocompatible. These crystalline rodlike particles have been derived from a variety of renewable sources including wood, cotton, ramie, bacteria, and tunicates (Eichhorn et al., 2010; Habibi, Lucia, & Rojas, 2010; Samir, Alloin, & Dufresne, 2005). Most importantly, CNCs with high crystallinity possess impressive mechanical properties. The modulus of CNCs determined by experimental and theoretical approaches are in the range of 100–160 GPa (Eichhorn et al., 2010). The majority of research on CNCs as a reinforcing material has focused on the bulk or thin film materials (Eichhorn et al., 2010; Habibi et al., 2010; Samir et al., 2005), whereas only a few studies have been reported recently on using CNCs as a reinforcing material for sub-micron polymer fibers fabricated by the electrospinning technique.

Electrospinning utilizes an external electrostatic field to generate small fibers with diameters on the sub-micron scale, and thus is widely used as an effective method to continuously produce nanofibers of polymers, ceramics and composites (Bhardwaj & Kundu, 2010; Dong, Nyame, Macdiarmid, & Jones, 2004; Dong, Wang, Sun, & Hinestroza, 2008; Huang, Zhang, Kotaki, & Ramakrishna, 2003). In the electrospinning process, a high voltage is applied to a polymer solution or melt, and electrostatic repulsion overcomes the liquid surface tension enabling the formation of fibers in non-woven mats or in one-dimensional aligned mats. Owing to their small fiber diameter, high surface-to-volume ratio and controllable porous structures, electrospun fibrous mats have

* Corresponding author. Tel.: +1 410 306 4398; fax: +1 410 306 0676.
E-mail address: hong.dong.ctr@mail.mil (H. Dong).

0144-8617/$ – see front matter © 2011 Elsevier Ltd. All rights reserved.
doi:10.1016/j.carbpol.2011.11.015

been studied for a variety of applications such as filtration, tissue engineering scaffolds, sensors, energy generation, drug delivery, and protective clothing (Bhardwaj & Kundu, 2010; Huang et al., 2003). To improve the mechanical properties of electrospun polymer fibers, nanofillers such as nanoclays (Li, Bellan, Craighead, & Frey, 2006) and carbon nanotubes (Chen, Liu, Zhou, Tjiu, & Hou, 2009; Hou et al., 2005; Ko et al., 2003) have been introduced into polymer solutions prior to electrospinning, and nanocomposite fibers were generated.

Continuous electrospun polymer nanofibers reinforced with nanostructured cellulose are of particular interest for more accurate assessments of the reinforcement capabilities of nanocellulose on a host polymer as well as for development of advanced fiber architectures. CNCs derived from ramie fibers (Peresin, Habibi, Zoppe, Pawlak, & Rojas, 2010; Zoppe, Peresin, Habibi, Venditti, & Rojas, 2009) or cellulose filter papers (Ping & Hsieh, 2009) or other sources have been reported to reinforce electrospun nanofibers of polyvinyl alcohol (Peresin et al., 2010), poly(ε-caprolactone) (Zoppe et al., 2009), polyacrylic acid (Ping & Hsieh, 2009), and polylactide (Xiang, Joo, & Frey, 2009). Cellulose nanocrystals/cellulose core-in-shell nanocomposites were prepared using a co-electrospinning technique (Magalhães, Cao, & Lucia, 2009). The CNC contents in these polymer matrices were usually below 20 wt%. The mechanical properties of electrospun porous fiber mats were typically measured using dynamic mechanical analysis (Peresin et al., 2010; Zoppe et al., 2009) or Instron tensile tests (Ping & Hsieh, 2009; Xiang et al., 2009). To the best of our knowledge, the nanomechanical investigation of individual sub-micron fibers of polymer reinforced with CNCs has not been previously reported. To eliminate the influence of thickness, porosity, distribution and intersection of fibers in the mats on mechanical properties of individual electrospun composite fibers, it is of fundamental interest to directly investigate the nanomechanical properties of single polymer and composite fibers.

Indentation properties of fibers have been investigated in various ways including: transverse indentation of fiber mats (Stanishevsky, Chowdhury, Chinoda, & Thomas, 2008; Thomas et al., 2006; Vondran, Sun, & Schauer, 2008), and axial (radial) nanoindentation of large (tens of microns) (Cayer-Barrioz, Tonck, Mazuyer, Kapsa, & Chateauminois, 2005; García-Leiva, Ocaña, Martín-Meizoso, & Martínez-Esnaola, 2002) and small (micron-sized) (Wang, Jin, Kaplan, & Rutledge, 2004) single fibers. Two studies in particular focus on transverse single fiber (or single wire) indentation of ZnO and related nano-wire structures (Chen, Zheng, Mao, & Li, 2010; Feng, Nix, Yoon, & Lee, 2006). Some studies take into account specific indenter and fiber geometries or boundaries which are encountered (Jakes et al., 2009). Specific studies have been done with nanoindentation of polymeric fibers in the transverse indentation direction for large diameter (several microns) fibers (Kamath, Ruetsch, Petrovicova, Kintrup, & Schwark, 2002) and small diameter (sub-micron) polymeric fibers (Tan & Lim, 2005). The current study encompasses many of these challenges and presents nanoindentation methods and nano-DMA analysis for sub-micron composite fibers using an instrumented nanoindenter.

Herein, we study wood-based CNC reinforcement on poly(methyl methacrylate) (PMMA), a glassy polymer with excellent transparency and good processing ability. Sub-micron nanocomposite fibers and their thermal and mechanical properties are reported here in a series of contents from 0% up to 41 wt% CNCs in PMMA. We also use electron microscopy to directly show the alignment of CNCs along the electrospun fiber axis, which provides a possible route towards aligning CNCs in bulk composites by using aligned fibers as a basis. Moreover, we used nanoindentation techniques to directly investigate nanoscale dynamic mechanical properties of the composite fibers and assess CNC reinforcement capabilities in PMMA as well as address some of the constraints relevant to performing nanoindentation on sub-micron fibers.

2. Experimental

2.1. Cellulose nanocrystals by sulfuric acid hydrolysis

Cellulose nanocrystals were prepared using a modification of the procedure reported by Gray et al. (Beck-Candanedo, Roman, & Gray, 2005). 300 g of a commercial grade softwood dissolving pulp were treated with 2.5 L of 64 wt% sulfuric acid at 45 °C for 60 min. The starting pulp suspension disintegrated rapidly to provide a white/gray slurry with low viscosity. The acid suspension was poured into 850 L of deionized water, combining 10 total reactions, and neutralized with sodium hydroxide. This was allowed to sit overnight for the solids to settle. The dilute salt and sugar solution was decanted off the top. After decanting, the solids were again slurried in 200 L of DI water and pumped through a membrane filtration system using a 200,000 Dalton cutoff PVCF membrane. Glucose and sodium sulfate were removed using multiple passes of dilution and filtration until sufficient purity was obtained. The suspensions were centrifuged in a Sharpel's continuous centrifuge to remove dirt and larger pulp particles that did not break up into single crystals. Crystals were concentrated to 6.32 wt% dispersion in water and stored in a cold room until needed. The typical product yield was between 100 and 150 g for a 300 g reaction (33–50%), or 1–1.5 kg for the combined ten reactions.

2.2. Dispersion of CNCs in DMF by solvent exchange

CNCs dispersed in H_2O were solvent-exchanged into a *N*,*N*-dimethylformamide (DMF) dispersion by vacuum-assisted rotary evaporation. A 150 mL aqueous dispersion of CNCs was poured into a round bottom flask, and 150 mL of DMF was added under agitation. Water and a small portion of DMF in the mixture were subsequently evaporated using the rotary evaporator until the amount of distillate was around 170 mL. The weight percentage of CNCs in DMF thus prepared was determined based on the dried weight of CNCs after evaporating solvent under vacuum for several days.

2.3. Electrospinning of PMMA and CNC/PMMA fibers

To prepare solutions of CNC/PMMA for electrospinning, PMMA (Sigma–Aldrich, Mw 350,000) was dissolved in DMF, and the requisite amount of CNCs in a DMF dispersion of known concentration was added to obtain the desired CNC weight percentage in the subsequent CNC/PMMA fibers. The concentrations of PMMA in the final solutions were calculated using the weights of solid PMMA and the volumes of DMF delivered from PMMA in DMF solutions and the CNC dispersion. For the studies of fiber morphology and thermal properties, the resultant concentrations of PMMA included 100 mg/mL, 90 mg/mL, 80 mg/mL, 70 mg/mL, 60 mg/mL, 50 mg/mL, 40 mg/mL corresponding to weight percentages of CNCs in the fibers at 0%, 5%, 9%, 17%, 23%, 33% and 41%, respectively. These solution concentrations were found to be suitable for producing ultra thin and uniform fibers at each CNC content. For nanomechanical studies, the concentrations of PMMA in solutions of 23%, 33% and 41% CNC/PMMA were adjusted to 65 mg/mL, 55 mg/mL and 55 mg/mL, respectively, so that the fibers of PMMA and CNC/PMMA produced at various CNC percentages achieved similar diameter ranges.

Fibers from solutions of PMMA with or without CNCs were generated by horizontal electrospinning. During the electrospinning

process, the polymer solution was stored in 10 mL plastic disposable syringes with 20 gauge needles, and the flow was controlled at a rate of 1 mL/h using a syringe pump. A positive voltage of 20 kV was applied to the needle, and a negative voltage of 3 kV was applied to aluminum foil as a collector that is 20 cm in distance apart from the needle. The electrospinning process was performed at an environment with a relative humility level of 25–40%. For aligning the fibers in one-dimension, a rotating mandrel covered with aluminum foil at a speed around 4500 rpm was used as a conductive collector.

2.4. Instrumentation

Scanning electron microscopy (SEM). The morphologies and diameters of the PMMA and CNC/PMMA fibers were examined using a Hitachi S-4700 scanning electron microscope at an accelerating voltage of 5 kV. The fiber samples were sputter-coated to reduce charging before SEM operation. To investigate the orientation of CNCs in the CNC/PMMA fibers, several drops of THF were dropped carefully to the fiber mats supported on aluminum foil to dissolve away the PMMA phase.

Transmission electron microscopy (TEM). The CNC specimen was examined by TEM using a Philips CM120 scanning transmission electron microscope at the University of Wisconsin Medical School Microscopy Laboratory. An electron beam potential of 80 kV was used; this provides better image contrast than higher beam energy. The suspension of CNCs in H_2O was diluted to 0.001%. A drop (~2–3 μL) of the diluted suspension was applied to a 3 nm thick carbon film which was supported by a thicker holey carbon film over a copper electron microscope grid. The ultra-thin carbon support film was employed to enhance the image contrast. The specimen was dried in a dust free environment. The measurements of CNC length and diameter were taken from the TEM image using ImagJ software, and 20 data points were collected on each measurement. Same method was applied to measure the diameters of the electrospun fibers from the SEM images.

Fourier transform infrared spectroscopy (FTIR). FTIR spectra of the freeze-dried CNCs, the PMMA fibers and the CNC/PMMA fibers at various percentages of CNCs were collected on a Thermo Nicolet NEXUS 870 spectrometer. The fiber samples were dried under vacuum and low heat. Sample pellets were prepared by grinding and pressing KBr powder with the fiber samples. The spectra were acquired in transmission mode on the sample pellets at a spectral range of 4000–500 cm^{-1}. 32 scans at a spectral resolution of 2 cm^{-1} were accumulated to achieve an adequate signal-to-noise ratio.

Differential scanning calorimetry (DSC). The thermal transitions of the fiber samples were characterized using a TA DSCQ1000 differential scanning calorimeter. The tests with sample weights of 6 mg each were carried out at a ramping rate of 10 °C/min from −40 °C to 200 °C under a N_2 atmosphere. The specimens were pre-dried under vacuum before DSC scans.

Thermogravimetric analysis (TGA). TGA was performed on a TA TGAQ5000 thermoanalyzer at a heating rate of 10 °C/min. Typically, samples with a weight between 8 mg to 15 mg were put in a platinum pan and heated from room temperature to 600 °C under a N_2 atmosphere.

2.5. Nanomechanical study of single fibers by nanoindentation

Nanoscale dynamic mechanical analysis (nano-DMA) was performed using a TI-950 TriboIndenter (Hysitron) equipped with a 500 nm radius, 60° conical probe. The tip area function for the probe was optimized for depths below 200 nm. Fibers were imaged at 0.40–0.65 μN imaging force to obtain fiber diameter prior to indentation tests. Nano-DMA testing was then performed with the probe centered on the fiber. The load function was load-controlled, ranging from 1 to 500 μN DC-load, where this ramp consisted of 50 equally spaced steps. The load started at 1 μN and increased, at a rate of 10 μN/s to the next DC-load. Holding at this DC-load, a 50 Hz dynamic load of 1 μN was applied, resulting in a dynamic displacement amplitude of typically 0.5–1.0 nm. After the dynamic load measurement, the DC-load again increased at a rate of 10 μN/s to the next equally spaced step-load and so on. Drift was measured at the initial preload of 1.0 μN for 20 s prior to each indent and correction was applied to the displacement data. Indentations were performed at multiple positions and on multiple fibers at each concentration.

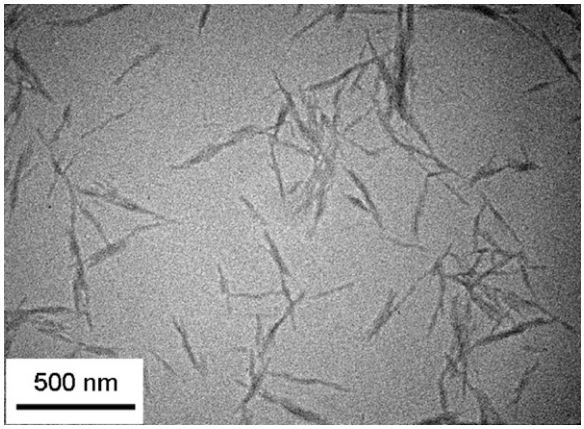

Fig. 1. Transmission electron micrograph of cellulose nanocrystals from water dispersion.

The storage modulus of CNC/PMMA fibers at different CNC contents was analyzed by the dynamic nanoindentation technique, which is used to obtain quantitative viscoelastic information from polymers at the nanoscale. The number of locations tested per sample ranged from 2 to greater than 13. An average of 8 data points per CNC content was used to determine the mean and standard deviation of the nano-DMA storage modulus (E') data.

3. Results and discussion

3.1. CNCs and dispersion in solutions prior to electrospinning

Cellulose nanocrystals were produced from wood pulp, an easily accessible and abundant natural source. The pulp fibers were disintegrated, and the amorphous regions of fibrils were hydrolyzed with sulfuric acid leaving nano-sized cellulose needles (Beck-Candanedo et al., 2005). The as-isolated CNC suspension was a stable aqueous dispersion, owing to electrostatic repulsion between cellulose nanocrystals. This electrostatic repulsion arises from negatively charged sulfate groups introduced by the sulfuric acid hydrolysis (van den Berg, Capadona, & Weder, 2007). Fig. 1 shows a representative TEM image of the morphology of wood-based CNCs produced by sulfuric acid hydrolysis. To overcome the low contrast of CNCs with the carbon support film in TEM imaging, a low voltage electron beam and ultra-thin carbon support film were used. The electron image was also slightly underfocused to enhance image contrast. A tendency of agglomeration could be observed from TEM sample preparation and image collecting, probably arising from drying of the suspension onto the carbon support film. The lengths (measured on the TEM image) of CNCs were in the 190–660 nm range (average 380 nm) while the average width is 17 nm with some tapering evident towards the ends of the nanocrystals.

Solution-based processing of nanocomposites and composite nanofibers requires good dispersability of both the CNCs and the polymer in a common solvent. Suspensions of CNCs in some polar

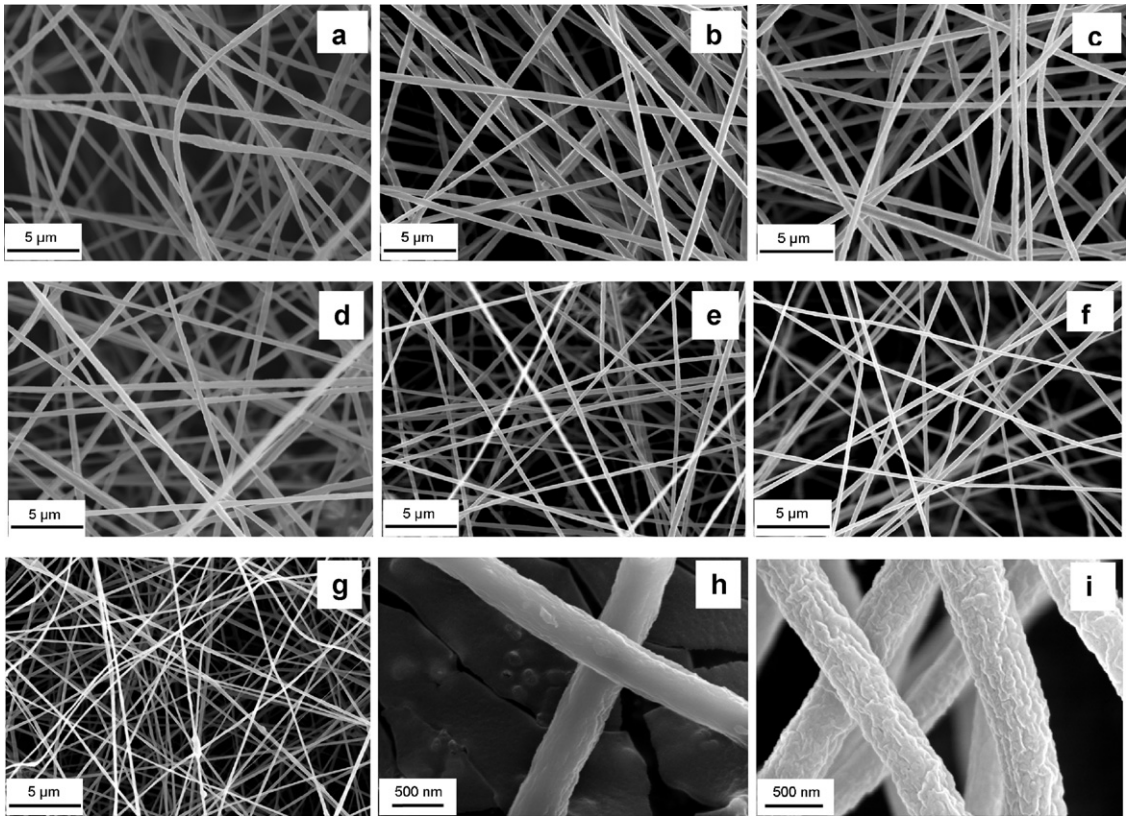

Fig. 2. Scanning electron micrographs of (a) PMMA fibers and (b–g) CNC/PMMA fibers at various w/w percentages of CNCs in fibers: (b) 5% CNC, (c) 9% CNC, (d) 17% CNC, (e) 23% CNC, (f) 33% CNC, (g) 41% CNC; (h) and (i) show fiber surface morphology of PMMA (h) and 17% CNC/PMMA (i).

organic solvents such as DMF could be produced via freeze-drying and subsequent redispersion under sonication. However, the fraction of redispersed CNCs was quite low due to the hydrophilic nature of cellulose and the strong hydrogen bonding interactions between cellulose nanocrystals (Viet, Beck-Candanedo, & Gray, 2007). Weder et al. (Tang & Weder, 2010) reported a two-step solvent exchange method on extracting CNCs from water and dispersing in DMF: the aqueous dispersions of CNCs were solvent-exchanged with acetone to form gels; and the gels were dispersed in DMF, followed by elimination of acetone from the mixture by evaporation. In our case, CNCs dispersed in water were directly solvent-exchanged into DMF by addition of DMF to the CNC aqueous solution followed by vacuum rotary evaporation of water. The dispersion of CNCs in DMF diluted to 5 mg/mL is comparable to its water dispersion at the same concentration. Examination under two crossed polarizers showed flow birefringence of CNCs in H_2O and DMF dispersions at a concentration of 5 mg/mL, indicating that CNCs were well dispersed both before and after solvent exchange (van den Berg et al., 2007; Viet et al., 2007). The dispersion of CNCs was maintained after adding to the PMMA/DMF mixture.

3.2. Morphology and chemical characterization of CNC/PMMA fibers

The morphologies of CNC/PMMA fibers in the mats were examined using scanning electron microscopy (SEM). Fig. 2 shows typical SEM micrographs for fibers electrospun from pure PMMA and from PMMA with different weight percentages of CNCs in fibers. All of the polymer compositions considered in this study yielded uniform nanofibers. Smooth fibers of CNC/PMMA were even generated at a high CNC content: CNCs with 41% in total weight were incorporated into uniform fibers, and a continuous non-woven mat was easily formed. The average diameters of the PMMA fibers and the CNC/PMMA fibers with 5% CNC, 9% CNC, 17% CNC, 23% CNC, 33% CNC, 41% CNC are 459 nm, 474 nm, 450 nm, 431 nm, 280 nm, 269 nm and 182 nm, respectively (Fig. 2a–g). For nanomechanical studies, fibers containing different percentages of CNCs were also fabricated into similar diameters by adjusting the concentrations of PMMA in the mixtures as shown in Section 2 and thus the viscosity of the electrospun solution.

CNC/PMMA fibers were initially electrospun from dispersions of CNCs and PMMA in DMF that have the same PMMA concentration of 90 mg/mL at various CNC contents. However, at a high CNC content such as 41%, the dispersion of CNC/PMMA in DMF becomes very viscous, and uniform fiber mats could not be generated by electrospinning. In order to produce ultra-thin fibers and well-formed fiber mats at various CNC contents, the concentration of PMMA in DMF started with 90 mg/mL for 5 wt% CNC/PMMA and decreased to 40 mg/mL for 41 wt% CNC/PMMA (see Section 2 for details). The addition of CNCs was believed to increase the conductivity of the electrospinning solution due to the negative charges brought by sulfate groups on CNC surfaces (Peresin et al., 2010). Thus a low concentration of PMMA at a high percentage of CNCs could be used to produce smooth nanocomposite fibers, resulting in reduced fiber diameters. Fibers of 41 wt% CNC/PMMA were readily electrospun from a mixture containing 40 mg/mL PMMA without spinning issues. Additionally, good dispersion of CNCs in PMMA/DMF prior to electrospinning could also contribute to the formation of CNC/PMMA fibers at various CNC contents up to 41 wt%.

The fiber surface morphologies with and without incorporation of CNCs were characterized at a high magnification. As shown in Fig. 2h, the surface of a PMMA fiber is relatively smooth. On the other hand, a wrinkled surface with shapes and sizes similar to that of CNCs was observed at 17 wt% CNC/PMMA (Fig. 2i) and on nanocomposite fibers at other percentages of CNCs. CNCs

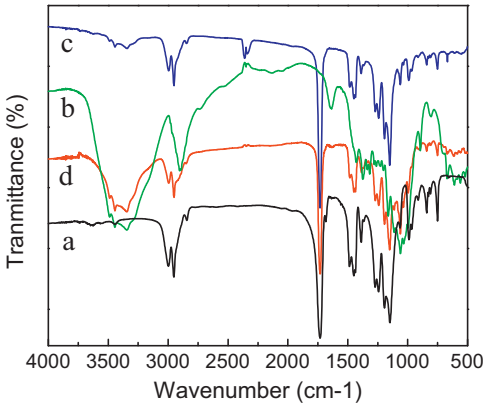

Fig. 3. FTIR spectra of (a) PMMA fibers, (b) freeze-dried CNCs, (c) 9 wt% CNC/PMMA fibers and (d) 33 wt% CNC/PMMA fibers.

were not observed to protrude from the outer fiber surface at any content.

To confirm the incorporation of CNCs in CNC/PMMA fibers, all the fiber mats were subjected to analysis with FTIR spectroscopy. Spectra of freeze-dried CNCs, PMMA fibers, 9 wt% CNC/PMMA fibers and 33 wt% CNC/PMMA fibers using as examples are presented in Fig. 3. Peaks corresponding to PMMA and CNCs were observed in the spectra of CNC/PMMA fibers. The FTIR spectra of CNCs, 9 wt% CNC/PMMA and 33 wt% CNC/PMMA showed broad bands in the range of 3500–3300 cm^{-1}, which are characteristic absorptions of the free hydroxyl and the hydrogen-bonded hydroxyl groups of cellulose. The typical carbonyl peak at 1731 cm^{-1} and other peaks corresponding to the matrix polymer PMMA were preserved in the spectra of 9 wt% and 33 wt% CNC/PMMA fibers. As the content of CNCs in composite fibers increases, the intensity of O–H bands relative to carbonyl peak increases.

3.3. Alignment of CNCs and the CNC/PMMA fibers

Alignment of electrospun fibers has been previously achieved by many techniques (Li & Xia, 2004), among which collection with a high-speed rotation mandrel is frequently used. By controlling the rotation speed of the mandrel, fibers of CNC/PMMA aligned along the rotation direction were obtained. The SEM image in Fig. 4a shows the morphology of one-dimensional aligned fibers of 33 wt% CNC/PMMA. The orientation of CNCs embedded in a CNC/PMMA fiber was investigated by solvent-etching PMMA from fibers with drops of THF. Interestingly, highly aligned CNCs were revealed along the fiber axis after etching, as displayed in Fig. 4b. The phenomena of orientation of nanofillers such as carbon nanotubes along the polymer fiber have been reported (Chen et al., 2009; Hou et al., 2005; Ko et al., 2003), in which functionalized carbon nanotubes were dispersed in the polymer solution prior to electrospinning. As suggested by Chen et al. (2009), the high alignment of nanofillers along the polymer fiber could be attributed to the following factors: the large electrostatic fields and the shear forces in the liquid jet during electrospinning; the nanoscale confinement effect; and the orientation of polymer chains during electrospinning.

3.4. Thermal properties of CNC/PMMA fibers

The thermal properties of PMMA fibers and CNC/PMMA fibers at different CNC contents were analyzed by DSC and TGA. As shown in Table 1, incorporation of low contents of CNCs into PMMA tends to increase the glass transition temperature (T_g) of PMMA. The T_g of pure PMMA is 119.5 °C. The T_g value of PMMA is increased to 123.3 °C with inclusion of 5 wt% CNCs, and further increased to 125.0 °C for 9 wt% CNC/PMMA fibers. Only minor changes in T_g are evident as the CNC content was increased above 9 wt%, with an apparent plateau at about 126.3 °C. A small increase of 3 °C in PMMA T_g was also reported on the fibers of PMMA with inclusion of microfibrils extracted from bacterial cellulose up to 3.5 wt%, whereas higher fraction of microfibrils showed a gradual decrease in PMMA T_g because of agglomeration of microfibrils as bundles in PMMA fibers (Olsson et al., 2010). In our study, T_g values of PMMA with high contents of CNCs showed a plateau without apparent decreasing, indicating high degree of dispersion of CNCs in PMMA fiber matrix.

Table 1
T_g data table from DSC for PMMA fibers and CNC/PMMA fibers.

Sample (fiber mat)	DSC T_g of PMMA (°C)
PMMA	119.5
5 wt% CNC/PMMA	123.3
9 wt% CNC/PMMA	125.0
17 wt% CNC/PMMA	125.2
23 wt% CNC/PMMA	126.3
33 wt% CNC/PMMA	125.9
41 wt% CNC/PMMA	126.5

The influence of CNCs on the thermal transitions of PMMA could be explained by interactions between the hydroxyl groups of CNCs and the carbonyl groups of PMMA. PMMA has an ester functional group ($COOCH_3$) in its side chain. This group can interact with abundant hydroxyl groups on the surface of CNCs through hydrogen bonding. Generally speaking, the presence of hydrogen bonds should raise the value of T_g because it restricts the motion of the polymer segments (Kuo, 2008). This is consistent with our DSC results on CNC/PMMA fibers. Hydrogen bonding interactions between hydroxyl and carbonyl groups have been widely used to facilitate miscibility of polymer blends (Kuo, 2008; Kuo & Chang, 2001), in which hydrogen bonding was found to have a significant effect on the thermal properties of polymer blends. The hydrogen bonding interactions between CNCs and PMMA could also facilitate the dispersion of CNCs in PMMA/DMF solutions.

Fig. 5 shows the weight loss and the corresponding derivative weight percent of PMMA fibers and CNC/PMMA composite fibers. CNCs show an onset of degradation at 247 °C and a maximal rate of mass loss at 303 °C, whereas the decomposition of PMMA fibers has a maximal rate of mass loss at 367 °C. Incorporation of CNCs into PMMA fibers yields curves indicating that degradation of the two materials occur as primarily separate events. Some offset of the PMMA degradation peaks (Fig. 5b) occurred after incorporating CNCs. The degradation temperature corresponding to the mass loss of PMMA increased from 367 °C for neat PMMA to 377 °C for PMMA with 5 wt% CNCs and to 381 °C for PMMA with 9 wt% CNCs. The degradation temperature of PMMA stabilized at slightly higher temperatures for samples with higher CNC contents, achieving 384 °C for PMMA with 41 wt% CNCs.

3.5. Nanomechanical properties of single fibers via nanoindentation

Fig. 6 shows examples of fibers after a shallow indent was performed (Fig. 6a) and after a deep indent was performed where the indenter probe approached the underlying glass substrate (Fig. 6b). Each fiber has a diameter on the order of 500 nm. These fibers were indented in the transverse direction to obtain stiffness properties.

Storage modulus (E') from the Nano-DMA measurements is shown in Fig. 7a. It suggests increasing storage modulus with the addition of CNCs up to at least 17 wt% CNCs. Further increases in CNC content did not appear to have significant impact on modulus. The average gain in modulus at 17 wt% CNCs compared to neat PMMA is approximately 0.9 GPa, which corresponds to a 17%

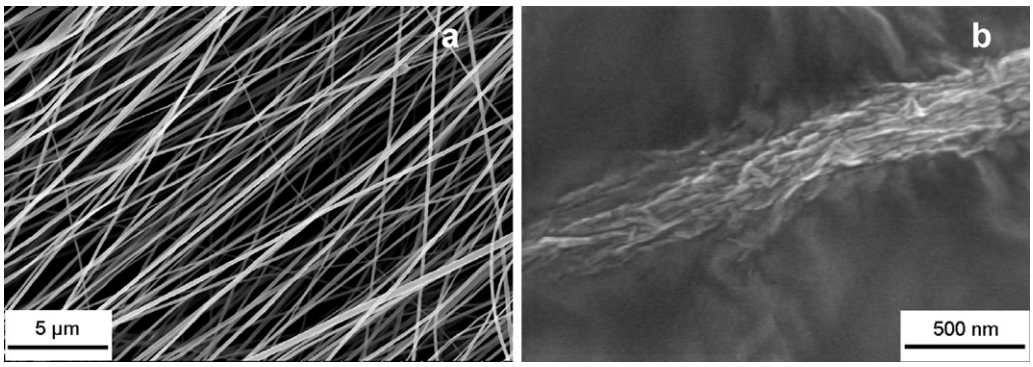

Fig. 4. Scanning electron micrographs of (a) alignment of 33 wt% CNC/PMMA fibers and (b) alignment of cellulose nanocrystals along fiber axis direction revealed by solvent etching.

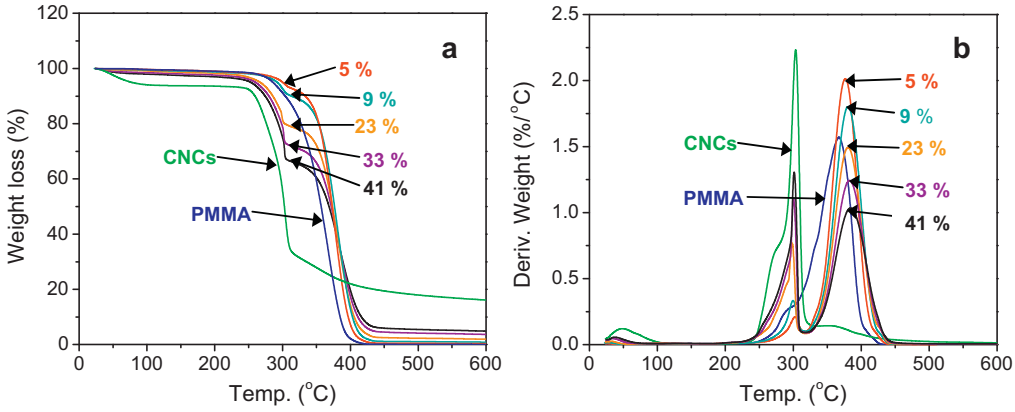

Fig. 5. TGA (a) and differential thermogravimetry (b) curves of PMMA, CNCs, 5 wt% CNC/PMMA, 9 wt% CNC/PMMA, 23 wt% CNC/PMMA, 33 wt% CNC/PMMA and 41 wt% CNC/PMMA.

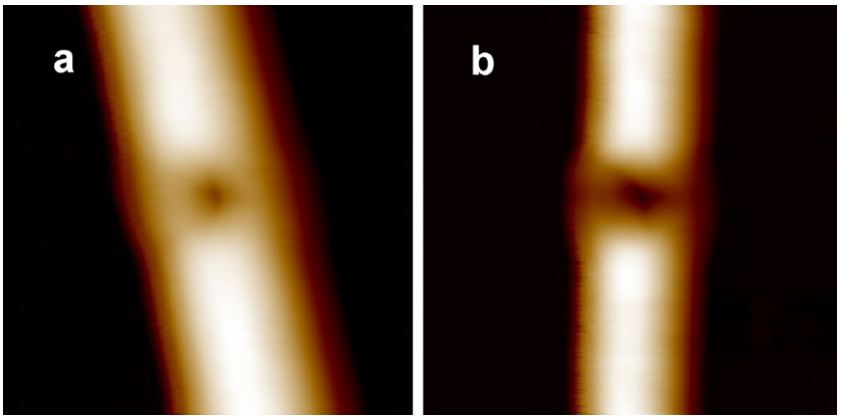

Fig. 6. Topographic images (4 μm × 4 μm, *x*–*y*) of (a) a fiber after a shallow indent was performed (1 μm light to dark) and (b) a fiber after a deep indent was performed (0.5 μm light to dark).

improvement. Because the indentation measurements are made in the transverse direction and the CNCs are largely aligned along the fiber axis, the actual increases in the axial modulus of the fiber with CNC content could be significantly larger than the measured 0.9 GPa improvement. Additional studies are required to measure axial and transverse fiber moduli independently to explore the level of anisotropy that is created with addition of CNCs. The modest increase in the storage modulus of PMMA fibers with incorporation of CNCs could also be attributed to the matrix PMMA as a glassy polymer has a high modulus of 5.4 GPa.

Obtaining reliable storage modulus values for sub-micron diameter fibers also requires consideration of the (1) effects of tip shape and surface location uncertainties on measurements at shallow depths (VanLandingham, Juliano, & Hagon, 2005), and (2) substrate effects that have been observed in thin films for indentation depths exceeding 10% of the overall film thickness (Fischer-Cripps, 2004). In order to analyze the data with minimal impact from these effects, modulus values arising from instrument artifacts were truncated (1) from the shallow depths (to reduce error arising from tip shape effects) and also (2) from the deep depths (to reduce error arising from substrate effects). Further, in order to compare fibers of slightly different diameters (the 55 fiber diameters used here averaged 508 ± 103 nm, and ranged from 326 nm to 798 nm), the indentation depth (h) was normalized to the fiber diameter (D), h/D,

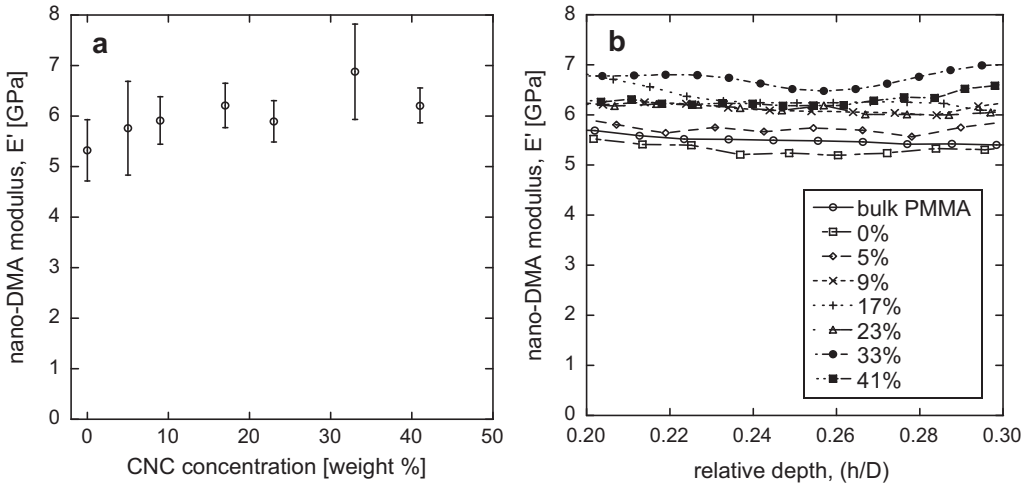

Fig. 7. (a) Nano-DMA storage modulus (E') data at various CNC contents. (b) Nano-DMA storage modulus data in the 20–30% relative depth (h/D) range for bulk PMMA film, PMMA fibers and CNC/PMMA fibers at each CNC content.

resulting in a relative depth. With the remaining normalized data for measurements corresponding to a given CNC content, a smoothing algorithm was applied. Fig. 7b shows the smoothed data of each CNC content for h/D in the 20–30% range (the actual average and standard deviation for this range is shown in Fig. 7a). For comparison, the modulus of a thick film (thickness ~2 mm) of neat PMMA is also plotted in Fig. 7b. In this case, the data were generated using the same load function, a similar amount of shallow depth data were discarded as for the fiber analysis, the indent depth was normalized to the maximum depth reached by the indenter (800 nm), and the same smoothing function was applied. The modulus value of the bulk PMMA matches that of the pure PMMA fiber in the 20–30% h/D range, suggesting that the issues arising from probe shape and sample depth effects have been adequately addressed with this analysis method.

The indentation methods presented here have dealt with some of the constraints found when performing nanoindentation on submicron fibers. Specific constraints that were identified include: (1) fiber diameter range and minimum, (2) depth to diameter ratio, and (3) valid depth range under these experimental conditions (diameter, material, load function). Finally, by making a comparison of the fiber results with those of a film, it was shown that the methods used here, including analysis of the data, are valid for the system studied. While these results do not necessarily extend to other systems, the importance of this work lies in enabling the study of single fiber indentation properties, especially for electrospun, sub-micron fibers. Measuring the modulus of a single fiber and relating that value to diameter and other properties allows the engineering of electrospun fiber mats with specific mechanical properties.

4. Conclusions

Cellulose nanocrystals derived from wood pulp fibers have been incorporated into electrospun PMMA fibers with weight up to 41%. Prior to electrospinning, CNCs were well dispersed both in processing solvent and in the mixture with PMMA. Uniform composite fiber mats containing various CNC contents were generated reproducibly with fiber diameters in the range of several hundreds of nanometers. The formation of CNC/PMMA fibers at high CNC percentages took account of factors such as low concentrations of PMMA solutions, conductivity increased with CNC contents and good dispersion of CNCs in PMMA/DMF. Nanocomposite fibers could be aligned using conventional electrospun fiber alignment techniques. The electrospinning process also facilitated alignment of CNCs along the fiber axis, making it feasible to use aligned electrospun fibers as an aid for CNC alignment in polymer composites. Thermal analysis revealed that the glass transition temperature of PMMA was increased with incorporation of CNCs, suggesting hydrogen bonding interactions between carbonyl in the ester groups of PMMA and hydroxyl groups on CNC surface. Nanoindentation study performed on these single sub-micron fibers in the transverse direction has been achieved. An analysis method has been determined that minimizes the effects from shallow indent depth (tip shape uncertainty) and deep indent depth (substrate stiffening effect). Single composite fibers investigated using nanoindentation techniques showed a modest increase in the mechanical properties with increasing CNC content, about 17% improvement in nano-DMA storage modulus with the first 17 wt% CNCs.

These studies present a method for incorporating evenly distributed CNCs into fibers, thin films and composites in a manner that facilitates CNC alignment. The demonstrated alignment of CNCs along the fiber long axis provides a new approach to orient CNCs with desired directions in polymer composites. For example, it may be feasible to achieve alignment of CNCs or whiskers in both thin film and bulk polymer composites through application of pressure at elevated temperature to layers of one-dimensional aligned nanocomposite fiber mats interspersed with the matrix polymer.

Acknowledgements

This research was supported in part by an appointment to the Postgraduate Research Participation Program at the U.S. Army Research Laboratory administered by the Oak Ridge Institute for Science and Education through an interagency agreement between the U.S. Department of Energy and USARL. The authors would like to acknowledge Dr. M.R. VanLandingham for insight and discussion on Nano-DMA work.

References

Beck-Candanedo, S., Roman, M., & Gray, D. G. (2005). Effect of reaction conditions on the properties and behavior of wood cellulose nanocrystal suspensions. *Biomacromolecules*, *6*, 1048–1054.

Bhardwaj, N., & Kundu, S. C. (2010). Electrospinning: A fascinating fiber fabrication technique. *Biotechnology Advances*, *28*, 325–347.

Cayer-Barrioz, J., Tonck, A., Mazuyer, D., Kapsa, P., & Chateauminois, A. (2005). Nanoscale mechanical characterization of polymeric fibers. *Journal of Polymer Science: Part B: Polymer Physics*, *43*, 264–275.

Chen, D., Liu, T. X., Zhou, X. P., Tjiu, W. C., & Hou, H. Q. (2009). Electrospinning fabrication of high strength and toughness polyimide nanofiber membranes containing

multiwalled carbon nanotubes. *Journal of Physical Chemistry B*, *113*, 9741–9748.
Chen, Y. Q., Zheng, X. J., Mao, S. X., & Li, W. (2010). Nanoscale mechanical behavior of vanadium doped ZnO piezoelectric nanofiber by nanoindentation technique. *Journal of Applied Physics*, *107*, 094302.
Dong, H., Nyame, V., Macdiarmid, A. G., & Jones, W. E. (2004). Polyaniline/poly(methyl methacrylate) coaxial fibers: The fabrication and effects of the solution properties on the morphology of electrospun core fibers. *Journal of Polymer Science Part B: Polymer Physics*, *42*, 3934–3942.
Dong, H., Wang, D., Sun, G., & Hinestroza, J. P. (2008). Assembly of metal nanoparticles on electrospun nylon 6 nanofibers by control of interfacial hydrogen-bonding interactions. *Chemistry of Materials*, *20*, 6627–6632.
Eichhorn, S. J., Dufresne, A., Aranguren, M., Marcovich, N. E., Capadona, J. R., Rowan, S. J., et al. (2010). Review: Current international research into cellulose nanofibres and nanocomposites. *Journal of Materials Science*, *45*, 1–33.
Feng, G., Nix, W. D., Yoon, Y., & Lee, C. J. (2006). A study of the mechanical properties of nanowires using nanoindentation. *Journal of Applied Physics*, *99*, 074304.
Fischer-Cripps, A. C. (2004). *Nanoindentation* (2nd ed.). New York: Springer.
García-Leiva, M. C., Ocaña, I., Martín-Meizoso, A., & Martínez-Esnaola, J. M. (2002). Fracture mechanics of Sigma SM1140+ fibre. *Engineering Fracture Mechanics*, *69*, 1007–1013.
Habibi, Y., Lucia, L. A., & Rojas, O. J. (2010). Cellulose nanocrystals: Chemistry, self-assembly, and applications. *Chemical Reviews*, *110*, 3479–3500.
Hou, H. Q., Ge, J. J., Zeng, J., Li, Q., Reneker, D. H., Greiner, A., et al. (2005). Electrospun polyacrylonitrile nanofibers containing a high concentration of well-aligned multiwall carbon nanotubes. *Chemistry of Materials*, *17*, 967–973.
Huang, Z. M., Zhang, Y. Z., Kotaki, M., & Ramakrishna, S. (2003). A review on polymer nanofibers by electrospinning and their applications in nanocomposites. *Composites Science and Technology*, *63*, 2223–2253.
Hussain, F., Hojjati, M., Okamoto, M., & Gorga, R. E. (2006). Review article: Polymer–matrix nanocomposites, processing, manufacturing, and application: An overview. *Journal of Composite Materials*, *40*, 1511–1575.
Jakes, J. E., Frihart, C. R., Beecher, J. F., Moon, R. J., Resto, P. J., Melgarejo, Z. H., et al. (2009). Nanoindentation near the edge. *Journal of Materials Research*, *24*, 1016–1031.
Kamath, Y. K., Ruetsch, S. B., Petrovicova, E., Kintrup, L., & Schwark, H.-J. (2002). Effects of spin finish on fiber surface hardness: An investigation with atomic force microscopy and frictional measurements. *Journal of Applied Polymer Science*, *85*, 394–414.
Ko, F., Gogotsi, Y., Ali, A., Naguib, N., Ye, H. H., Yang, G. L., et al. (2003). Electrospinning of continuous carbon nanotube-filled nanofiber yarns. *Advanced Materials*, *15*, 1161–1165.
Kuo, S. W. (2008). Hydrogen-bonding in polymer blends. *Journal of Polymer Research*, *15*, 459–486.
Kuo, S. W., & Chang, F. C. (2001). Miscibility and hydrogen bonding in blends of poly(vinylphenol-co-methyl methacrylate) with poly(ethylene oxide). *Macromolecules*, *34*, 4089–4097.
Li, D., & Xia, Y. N. (2004). Electrospinning of nanofibers: Reinventing the wheel? *Advanced Materials*, *16*, 1151–1170.
Li, L., Bellan, L. M., Craighead, H. G., & Frey, M. W. (2006). Formation and properties of nylon-6 and nylon-6/montmorillonite composite nanofibers. *Polymer*, *47*, 6208–6217.
Magalhães, W. L. E., Cao, X., & Lucia, L. A. (2009). Cellulose nanocrystals/cellulose core-in-shell nanocomposite assemblies. *Langmuir*, *25*, 13250–13257.
Olsson, R. T., Kraemer, R., López-Rubio, A., Torres-Giner, S., Ocio, M. J., & Lagarón, J. M. (2010). Extraction of microfibrils from bacterial cellulose networks for electrospinning of anisotropic biohybrid fiber yarns. *Macromolecules*, *43*, 4201–4209.
Peresin, M. S., Habibi, Y., Zoppe, J. O., Pawlak, J. J., & Rojas, O. J. (2010). Nanofiber composites of polyvinyl alcohol and cellulose nanocrystals: Manufacture and characterization. *Biomacromolecules*, *11*, 674–681.
Ping, L., & Hsieh, Y.-L. (2009). Cellulose nanocrystal-filled poly(acrylic acid) nanocomposite fibrous membranes. *Nanotechnology*, *20*, 415604.
Samir, M. A. S. A., Alloin, F., & Dufresne, A. (2005). Review of recent research into cellulosic whiskers, their properties and their application in nanocomposite field. *Biomacromolecules*, *6*, 612–626.
Stanishevsky, A., Chowdhury, S., Chinoda, P., & Thomas, V. (2008). Hydroxyapatite nanoparticle loaded collagen fiber composites: Microarchitecture and nanoindentation study. *Journal of Biomedical Materials Research Part A*, *86*, 873–882.
Tan, E. P. S., & Lim, C. T. (2005). Nanoindentation study of nanofibers. *Applied Physics Letters*, *87*, 123106.
Tang, L., & Weder, C. (2010). Cellulose whisker/epoxy resin nanocomposites. *ACS Applied Materials & Interfaces*, *2*, 1073–1080.
Thomas, V., Jose, M. V., Chowdhury, S., Sullivan, J. F., Dean, D. R., & Vohra, Y. K. (2006). Mechano-morphological studies of aligned nanofibrous scaffolds of polycaprolactone fabricated by electrospinning. *Journal of Biomaterials Science Polymer Edition*, *17*, 969–984.
van den Berg, O., Capadona, J. R., & Weder, C. (2007). Preparation of homogeneous dispersions of tunicate cellulose whiskers in organic solvents. *Biomacromolecules*, *8*, 1353–1357.
VanLandingham, M. R., Juliano, T. F., & Hagon, M. (2005). Measuring tip shape for instrumented indentation using atomic force microscopy. *Measurement Science and Technology*, *16*, 2173–2185.
Viet, D., Beck-Candanedo, S., & Gray, D. G. (2007). Dispersion of cellulose nanocrystals in polar organic solvents. *Cellulose*, *14*, 109.
Vondran, J. L., Sun, W., & Schauer, C. L. (2008). Crosslinked, electrospun chitosan–poly(ethylene oxide) nanofiber mats. *Journal of Applied Polymer Science*, *109*, 968–975.
Wang, M., Jin, H. -J., Kaplan, D. L., & Rutledge, G. C. (2004). Mechanical properties of electrospun silk fibers. *Macromolecules*, *37*, 6856–6864.
Xiang, C. H., Joo, Y. L., & Frey, M. W. (2009). Nanocomposite fibers electrospun from poly(lactic acid)/cellulose nanocrystals. *Journal of Biobased Materials and Bioenergy*, *3*, 147–155.
Zoppe, J. O., Peresin, M. S., Habibi, Y., Venditti, R. A., & Rojas, O. J. (2009). Reinforcing poly(epsilon-caprolactone) nanofibers with cellulose nanocrystals. *ACS Applied Materials & Interfaces*, *1*, 1996–2004.